IEEE 802.11ax: On Time Synchronization in Asynchronous OFDM Uplink Multi-User MIMO Physical Layer

Roger Pierre Fabris Hoefel

***Abstract*—The High Efficiency WLANs (HEW) Task Group (TG) has been developing since 2014 the IEEE 802.11ax amendment, the 6th generation of wireless local area networks (WLANs). One major novel feature of IEEE 802.11ax standard is the specification of uplink multi-user multiple-input multiple-output (UL MU-MIMO) techniques to cope with the increase of UL data/video traffic from small-form devices in ultra-dense networks. In this paper, we first show that the UL MU-MIMO physical layer performance can be dramatically impaired due to the asynchronous reception over the uplink channel. Next, we propose and evaluate the performance of a time advance mechanism designed for IEEE 802.11ax WLANs that mitigates adequately the performance loss due to asynchronous UL MU-MIMO channels.**

***Keywords*—802.11ax; Uplink Multi-User MIMO; Synchronization.**

I. INTRODUCTION

A first draft elaborated by the IEEE Task Group (TG) 802.11ax was proposed in March 2016 [1]. The TG 802.11ax has included multi-user (MU) transmissions in the 11ax Specification Framework Document (SFD) [2]. The uplink multi-user multiple-input multiple-output (UL MU-MIMO) scheme is an essential joint medium access control (MAC) and physical layer (PHY) protocol to improve the network throughput in ultra-dense wireless local area networks (WLANs) in usage cases where the networks are loaded with small form devices that are only capable of transmitting 1-2 spatial streams (SS) [3].

A simulation study on the susceptibility of orthogonal frequency division multiplexing (OFDM) UL MU-MIMO PHY performance with relation to (w.r.t.) differences in power, timing and carrier frequency offset (CFO) between the uplink clients was presented in [4] during the standardization of the IEEE 802.11ac amendment. Although, the 2013 IEEE 802.11ac spec has only defined a downlink (DL) MU-MIMO scheme.

We also have been analyzing the effects of hardware impairments on the performance of UL MU-MIMO 802.11ax WLANs. In [5] we show that a frequency domain CFO estimation scheme has a superior performance in relation to the time domain CFO estimation algorithm in the context of 802.11ax UL MU-MIMO PHY. The reference [5] aims at complementing the references [6] (where a three-stage CFO mitigation scheme was proposed) and [7] (where it was shown that the performance of the clients without CFO is not impaired due to the residual CFO that impinges the other clients).

In [8] we show that, besides on-chip calibration, additional counterbalance algorithms should be implemented to reduce substantially the non-linear effects of in-phase and quadrature (IQ) imbalance on the IEEE 802.11ax UL MU-MIMO PHY when realistic channel estimation schemes are considered.

Roger Pierre Fabris Hoefel, Department of Electrical Engineering, Federal University of Rio Grande do Sul (UFRGS), Porto Alegre, Rio Grande do Sul (RS), Brazil; E-mail: roger.hoefel@ufrgs.br.

The 802.11ax Project Authorization Request (PAR) aims at four times network throughput gain in relation to the 802.11ac spec. Simulation results presented by the industry in the 802.11ax TG meetings have indicated that four times throughput gain can be obtained by the UL MU-MIMO PHY [9]. Although, the effects of non- ideal aspects (e.g., CFO, time synchronization) on the system throughput were not investigated in [9]. Qualitatively remarks on the effects of time and frequency synchronization on UL MU-MIMO PHY performance were presented in [10] based on the simulation results shown in [4] during the specification of the IEEE 802.11ac amendment. Fundamentally, it was proposed in [10] that the TG 802.11ax align their time/frequency synchronization requirements with those ones specified by 3GPPP for Long Term Evolution (LTE) cellular systems.

This paper is organized as follows: Section II succinctly describes an IEEE 802.11ax PHY simulator. To the best of our knowledge, this is the first peer-review paper that investigates thoroughly the performance of the asynchronous OFDM UL MU-MIMO 802.11ax PHY over different scenarios, as we have carried out in Section III. Section IV proposes and evaluates a simple protocol designed to mitigate the effects of asynchronous UL MU-MIMO channel on the performance of IEEE 802.11ax WLANs. Finally, we present our conclusions in Section V.

II. IEEE 802.11AX SIMULATOR

We shall evaluate in this paper the system performance of an asynchronous UL MU-MIMO PHY using an IEEE 802.11ax simulator that we have been developing, as summarized in Tab. I [5]. Results that allow a first order validation of our simulator can be found in [5,8]. A description of the MIMO Least Squares (LS) channel estimation scheme can be found in [11, pp. 98].

Table I– Parameters of IEEE 802.11ax simulator. Acronyms: GI (Guard Interval); MCS (Modulation and Code Scheme).

Parameter	Value	Parameter	Value
Carrier Frequency	5.25 GHz	**MCS**	0-9
Bandwidth	20 MHz, 40 MHz, 80 MHz	**Number of Spatial Streams**	1 to 8
GI Length	800 ns	**Synchronization**	Auto-Correlation
Modulation	BPSK, QPSK, 16-QAM, 64QAM, 256-QAM	**MIMO Channel Estimation**	Least Squares (LS)
Binary Convolutional Code (BCC)	Code rate: r=1/2, r=2/3, r=3/4, r=5/6	**Channel Decoder**	Hard and Soft-Decision Viterbi Decoding

In this paper, we investigate the performance of UL MU-MIMO 802.11ax PHY for the modulation and code schemes (MCS) shown in Tab. II. Observe that six clients, transmitting simultaneously one SS per client, produces a total PHY rate of 1.755 Gbps when the MCS7 is used in a system with a bandwidth (BW) of 80 MHz. In the present research, we implement an interference cancellation minimum mean squared error (IC-MMSE) MU-MIMO detector [5,8].

Table II - MCS analyzed in this paper. The PHY data rates assume a guard-interval (GI) of 800 ns and BW of 80 MHz.

MCS	Mod	BCC Code Rate	# SSs/ # STAs	Data Rate per STA/ Total Data Rate
3	16-QAM	½	1/6	117/702 Mbps
7	64-QAM	5/6	1/6	292.5/1755 Mbps

Hereafter, the UL MU-MIMO channel defined as $[n_t,n_r,K,n_{ss}]$ have the following characteristics: *(i)* each station (STA) has an equal number of n_t transmit antennas; *(ii)* the access point (AP) has n_r receive antennas; *(iii)* the channel is loaded with K STAS; *(iv)* each STA transmits an equal number of n_{ss} SS.

III. Performance of UL MU-MIMO 802.11ax PHY

A. Asynchronous Uplink OFDM MU-MIMO Channel

First, the PHY time synchronization scheme implemented in our IEEE 802.11ax simulator is described to ease a clear understanding of the interrelations between the asynchronous OFDM UL MU-MIMO channel and the system performance.

Fig. 1 shows the legacy preamble specified in the IEEE 802.11a/g/n/ac/ax amendments [11-13]. The first field transmitted in the IEEE 802.11ax frame is the legacy short training field (L-STF), which is carefully designed to have a low peak-to-average power ratio (PAPR) to avoid the non-linear effects in the analog-to-digital conversion (ADC), given that the L-STF is first used to implement automatic gain control (AGC). After implementing the AGC, the L-STF is utilized to implement temporal synchronization and coarse estimation of the CFO [5]. The L-STF transports 10 repetitions of a known short symbol with period of $P_{L\text{-}STF}$ (e.g., $P_{L\text{-}STF}$ is equal to 64 when the BW is set to 80 MHz). The legacy long training field (L-LTF) has *2* repetitions of a long symbol plus an extended cyclic prefix $CP_{L\text{-}LTF}$. The extended CP implemented in the L-LTF allows more robustness to the channel delay spread since the L-LTF is used to perform channel estimation and to refine the gross CFO estimated at the L-STF [5]. Assuming a BW of 80 MHz, then the length of each L-LTF $P_{L\text{-}LTF}$ has 256 samples and the extended cyclic prefix $CP_{L\text{-}LTF}$ has 128 samples [11-12]. The short and long CP used in control and data OFDM symbols of IEEE 802.11ac/ax frames have 32 (400 ns) and 64 samples (800 ns), respectively, when a BW 0f 80 MHz is used.

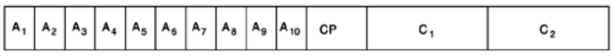

Figure 1. The legacy preamble used in IEEE 802.11a/g/n/ac/ax WLANs. For the IEEE 802.11ac/ax amendments using a BW of 80 MHz then A_1-A_{10} are periodic pilots with period of 64 samples per symbol; CP is an extended cyclic prefix with 128 samples and C_1-C_2 are periodic pilots with 256 samples per symbol.

There is a lack of channel state information (CSI) during the time-frequency synchronization period. Therefore, the input symbols to the synchronization scheme are obtained using an equal gain combining (EGC) scheme, i.e.,

$$y[n] = \sum_{j=1}^{n_r} r_j[n], \quad (1)$$

where n_r is the number of receive antennas and $r_j[n]$ is the *n*th sample of the symbol received at *j*th antenna.

The synchronization time θ is estimated using the L-STF according with the following expression [14-15]:

$$\theta = \max_n \left(\frac{|c_n|^2}{(p_n)^2}\right) = \max_n \left(\frac{\left|\sum_{m=0}^{L-1} y_{n+m}^* \, y_{n-P_{L-STF}+m}\right|^2}{\sum_{m=0}^{L-1} |y_{n+m}|^2)^2}\right), \quad (2)$$

where the parameter L is equal to or multiple of $P_{L\text{-}STF}$. In this paper, we have utilized L=576 since 9 short symbols of the L-STF are used, where each short symbol of the L-STF has 64 samples when the BW is set to 80 MHz. Notice that the numerator of (2) implements the autocorrelation of the received samples with the samples delayed by the L-STF length of each short L-STF symbol. The denominator of (2) estimates the received power to normalize the auto-correlation in order to diminish its dependence with the received power changes due to the multipath fading channel.

The interrelations between the probability distribution function (PDF) of the estimated synchronization time θ and the range of discrete time transform (DFT) implemented in the receiver of a generic OFDM based PHY are depicted in Fig. 2.

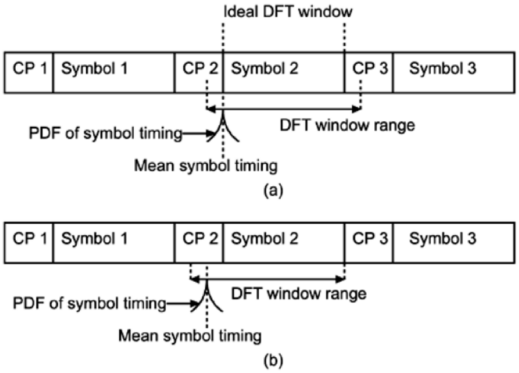

Figure 2. Effects of synchronization inaccuracies in the DFT window range in OFDM based modems [13, pp. 61].

Figure 2a shows that the inaccuracies in the estimated synchronization time can cause both inter-carrier interference (ICI) and inter-symbol interference (ISI) since the DFT window range for *m*th OFDM symbol includes the CP of the next OFDM symbol. Although, Fig. 2b shows that both ICI and ISI can be avoided if a proper delay in the estimated synchronization time is implemented. Therefore, the synchronization time estimated using (2) is redefined as follows:

$$\hat{\theta} = \theta + \Delta\theta. \quad (3)$$

The relation between the synchronization delay in samples $\Delta\theta$ and the synchronization delay in seconds $\Delta\tau$ is given by

$$\Delta\theta = \frac{\Delta\tau}{T_s} = \Delta\tau \cdot BW, \quad (4)$$

where T_s is the sample interval used in the OFDM PHY. For instance, assuming the typical BW of 80 MHz used in IEEE 802.11ac/ax WLANs, then the sample period T_s is equal to 12.5 ns (1/BW) and, therefore, 20 samples correspond to a synchronization delay of 250 ns.

The imperfect time synchronization introduces a phase offset when the DFT is applied to the received sequence, i.e.,

$$DFT\{y[n-\hat{\theta}]\} = Y[k] \cdot e^{-i\frac{2\pi k}{N_{DFT}}\hat{\theta}} = Y[k]e^{-i\phi}, \quad (5)$$

where N_{DFT} and *Y[k]* denote the DFT length and the symbol transmitted in the *k*th subcarrier (SC), respectively. However, if there is no ICI and ISI, as shown in Fig. 2b, then this phase offset ϕ can be mitigated using the pilot symbols transported in the L-LTF [15].

B. Asynchronous Canonical UL MU-MIMO Channel

In this paper, the asynchronous reception over UL MU-MIMO channels is modelled assuming that half of the clients have ΔT

ns extra delay relative to the other half [4], i.e., the typical model specified in the TG 802.11ax to assess the effects of asynchronous channel on the performance of OFDM UL MU-MIMO PHY is implemented in our IEEE 802.11ax simulator.

Fig. 3 shows the medium access control protocol data unit (MPDU) packet error rate (PER) as a function of the signal-to-noise ratio (SNR) given in decibels (dB), where the results are parameterized by the channel delay ΔT and the sample delay $\Delta\theta$ utilized in the time synchronization scheme. The canonical [1,8,6,1] UL OFDM MU-MIMO channel is simulated, defined as a flat fading Rayleigh channel independent and identically distributed (i.i.d.) among the clients as well as i.i.d. among the receive antennas. These results also assume perfect channel state information (CSI) and MCS7 *(64-QAM, BCC with code rate r=5/6)*. In this paper, we define perfect CSI when the additive zero-mean circular symmetric complex Gaussian (ZMCSCG) noise is neglected during the synchronization and channel estimation and, therefore, the noise only affects the detection of data symbols transmitted in the MPDU payload.

Analyzing the results shown in Fig. 3, we can infer the following conclusions: *(i)* there is no performance loss if the synchronization delay $\Delta\theta$ can cope with the channel delay without introducing ICI and ISI, cf. the results shown for $(\Delta T, \Delta\theta) = (300\ ns, 350\ ns)$; $(\Delta T, \Delta\theta) = (400\ ns, 400\ ns)$; *(ii)* there is a severe performance loss if the synchronization delay $\Delta\theta$ is not big enough to handle the channel delay, cf. results depicted for $(\Delta T, \Delta\theta) = (300\ ns, 250\ ns)$; *(iii)* there is a dramatic performance loss if the sum of the synchronization delay $\Delta\theta$ with the channel delay is greater than the CP length, cf. results depicted for $(\Delta T, \Delta\theta) = (400\ ns, 450\ ns)$. Notice that the CP has a length of 800 ns when the long guard period (GP) is implemented in IEEE 802.11ac/ax WLANs.

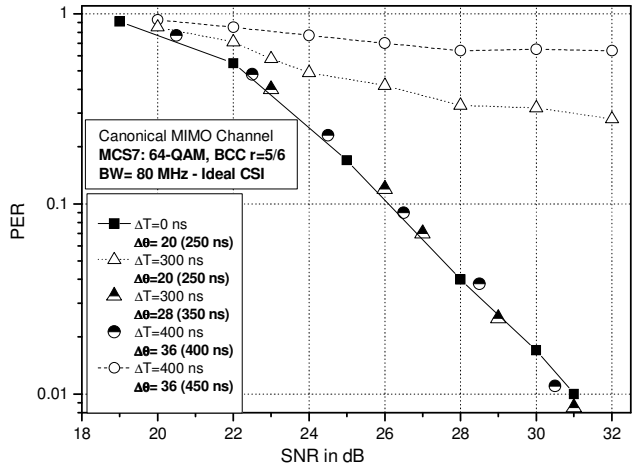

Figure 3. Interrelations between the asynchronous reception and synchronization delay on the MPDU PER as a function of SNR in dB: [1,8,1,6] canonical UL MU-MIMO channel; BW=80 MHz; MU-MMSE receiver with perfect CSI; MPDU payload of 1500 bytes; soft-decision Viterbi decoding.

Figure 4 shows the input signal to the synchronization algorithm and the signal generated at the output of the auto-correlation synchronization algorithm. It is assumed the same set up utilized in Fig. 3, particularized for a SNR of 32 dB. In both Figures 4a and 4b, the reception of the signal transmitted by the non-delayed and delayed clients starts at samples 1000 and 1036 (i.e., a delay of 450 ns), respectively. Notice that there is only noise until de sample 999, which allows to stress the capability of the synchronization scheme to detect the incoming transmissions. Analyzing the waveforms shown in the upper graphics Figures 4a and 4b, we can verify the ten periodic repetitions of the L-STF, cf. schematized in Fig. 1. Fig. 4a shows that the synchronization occurs at sample 1036, since in this channel realization the delayed clients present more power than the non-delayed ones. On the other hand, Fig. 4b shows that in another channel realization, the synchronization happens at sample 1000 due to the higher received power of the non-delayed clients in this channel realization.

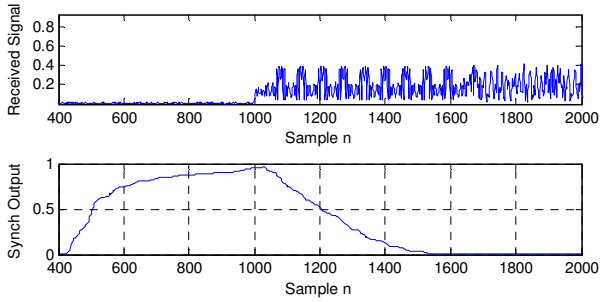

Figure 4a. Channel realization where the synchronization occurs at the time epoch of the delayed clients (sample #1036).

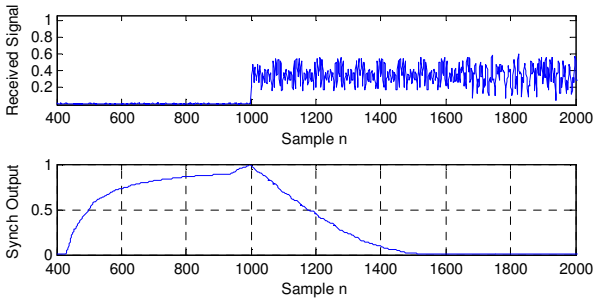

Figure 4b. Channel realization where the synchronization occurs at the time epoch of the non-delayed clients (sample #1000).

Figure 4. Received signal used as input for the time synchronization algorithm and the output of the synchronization algorithm: [1,8,6,1] canonical UL MU-MIMO, where the clients 1 to 3 have a delay of 1000 samples and the clients 4 to 6 have an extra delay of 36 samples (450 ns), SNR of 32 dB.

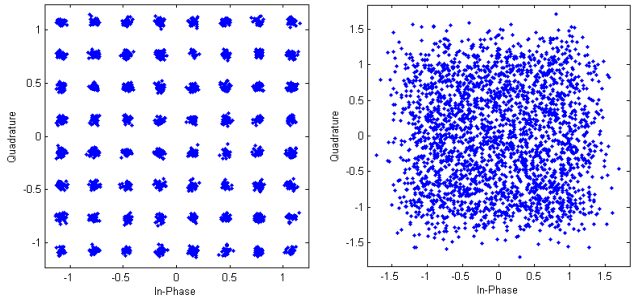

Figure 5. Received constellation of 64-QAM symbols at MU-MMSE MIMO detector output when the symbols are transmitted over the [1,8,6,1] canonical UL MU-MIMO channel with a SNR of 32 dB, channel delay ΔT of 400 ns and synchronization delay $\Delta\theta$ of 450 ns: (a) constellation of one *delayed client* when the synchronization occurs at the time arriving of the **delayed clients** (cf. Fig. 4a); (b) constellation of one *delayed client* when the synchronization occurs at the time epoch of the ***non-delayed clients*** (cf. Fig. 4b).

Fig. 5 shows the scatter diagram of the constellation of received symbols at the output of the MU-MMSE MIMO detector. Fig. 5a shows, without losing the generality, the received constellation of one *delayed client* that corresponds to the synchronization case shown in Fig. 4a, where the frames of both non-delayed and delayed clients can be detected and decoded without ICI and ISI. Notice that in this study case: *(i)* the CP and decoded samples for the *non-delayed clients* start at

samples 972 (1000-64) and 1000 (1036-36), respectively; *(ii)* the CP and decoded samples for the *delayed clients* start 972 (1036-64) and 1000 (1036-36), respectively. In summary, in this particular case the CP protects both non-delayed and delayed clients from ICI and ISI.

On other hand, Fig. 5b shows, without losing the generality, that the constellation of one *delayed client* is highly spread due to ICI and ISI, which corresponds to a high PER as shown in and SNR equal to 32 dB. Fig. 3, i.e., a PER of 64% for $(\Delta T, \Delta\theta) = (400\ ns, 450\ ns)$. Notice that in this study case, the CP and decoded sample for the *non-delayed clients* start at samples 936 (1000-64) and 964 (1000-36), respectively. Hence, the CP is large enough to protect the symbols from ICI and ISI. On the other hand, for the *delayed clients* the CP and decoded sample start at samples 972 (1036-64) and 964 (1000-36), respectively. Therefore, in this last case the CP is not large enough to prevent ISI and ICI for the non-delayed clients.

C. Asynchronous TGac B UL MU-MIMO Channel

The TGac B channel model, which models intra-room and room-to-room in residential environments, has a maximum excess delay of 90 ns and root mean square (rms) delay spread of 15 ns. It is a spatial correlated channel at both transmit and receive sides, having impulsive response with two overlapping clusters with 5 and 7 taps, respectively [11, pp. 39, pp. 57].

Figures 6a and 6b show the SNR as function of SNR in dB for MCS3 (16-QAM) and MCS7 (64-QAM), respectively, where the TGac B [1,8,6,1] UL MU-MIMO channel is assumed. Analyzing the Fig. 6a, we can infer the following interesting conclusions: *(i)* for both ideal CSI and Least Squares (LS) CSI there is a negligible performance degradation when the channel delay ΔT is set to either 200 ns or 300 ns if the auto-correlation synchronization scheme uses a delay $\Delta\theta$ of 350 ns; *(ii)* assuming a PER of 1%, there is a power loss of 5 dB for the configuration $(\Delta T, \Delta\theta) = (400\ ns, 400\ ns)$ due to ISI and ICI, even this channel having a small rms delay spread of 15 ns; *(iii)* there is a power loss of approximately 3 dB due to the realistic LS CSI.

The results shown in Fig. 6b allow similar conclusions in relation to Fig. 6a, except that now the configuration $(\Delta T, \Delta\theta) = (400\ ns, 400\ ns)$ impinges a substantial power loss (i.e., a PER of 40% for a SNR of 36 dB is observed). Notice the 64-QAM signaling scheme is much more susceptible to ICI and ISI than the 16-QAM scheme, which explains the dramatic degradation in the MPDU PER when $\Delta T = 400\ ns$.

D. Asynchronous TGac D UL MU-MIMO Channel

The TGac D channel model, which represents sea of cubes and large conference rooms in typical office environments, has a maximum excess delay of 390 ns and rms delay spread of 50 ns. It is a spatial correlated channel at both transmit and receive sides and it has impulsive response with three overlapping clusters with 16, 7 and 4 taps, respectively [11, pp. 39, pp. 58].

Figure 7 shows the PER as function of SNR in dB for MCS3 (16-QAM), where the TGac D [1,8,6,1] UL MU-MIMO channel is simulated. First, we can see that the system performance is completely degraded when the channel delay ΔT is set to *400 ns*. Note that this difference in relation to Fig. 6a (where a power loss of 5 dB was seen) occurs due to the higher delay spread of the TGac D channel (*50 ns*) in relation

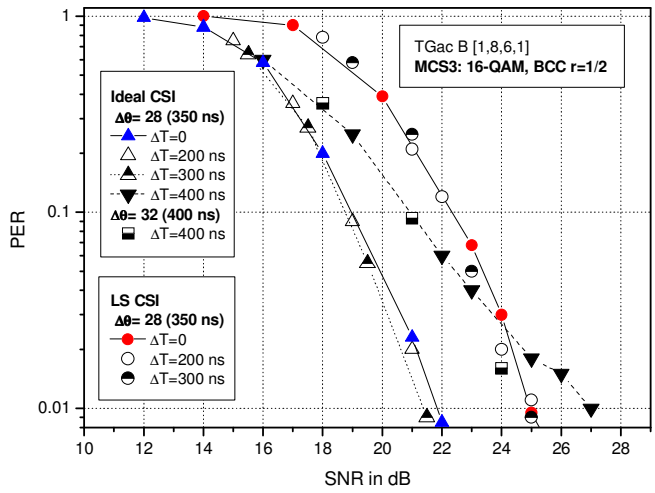

Figure 6a. MCS3: 16-QAM, BCC with r=1/2.

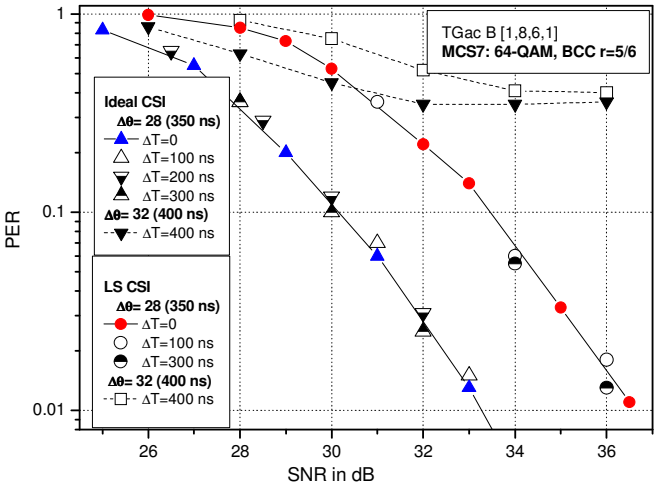

Figure 6b. MCS7: 64-QAM, BCC with r=5/6.

Figure 6. Effects of asynchronous reception on the PER: [1,8,6,1] TGac B channel; BW=80 MHz; MU-MMSE receiver with LS CSI, MPDU payload of 1500 bytes; soft-decision Viterbi decoding.

to the TGac B channel (*15 ns*). However, a non-expected difference w.r.t the results shown in Fig. 6b has been observed in Fig. 7, i.e., there is a performance improvement of 1 dB when the delayed users have a latency of either *200 ns* or *300 ns* in relation to the non-delayed clients. The TGac D channel is a very demanding channel to the MMSE MU-MIMO detector since it is a highly frequency selective with spatial correlation [5]. Hence, we believe that the temporal delay that can be absorbed by the CP length increases the orthogonality between the clients and, consequently, increasing the performance of the MMSE MU-MIMO detector.

IV. TIME ADVANCE SCHEME FOR THE IEEE 802.1AX UL MU-MIMO PHY

We assume that the Trigger Frame (TF) transmitted from the AP to the STAs scheduled to the next UL MU-MIMO transmission, as shown in Fig. 8, contains a field that indicate the time advance that must be used for each client in the transmission of the next UL MU Data frame. In the IEEE 802.11 WLANs, each STA in the basic service set (BSS) has a timer synchronized with the *timing synchronization function (TSF)* of every other STA associated in the BSS managed by

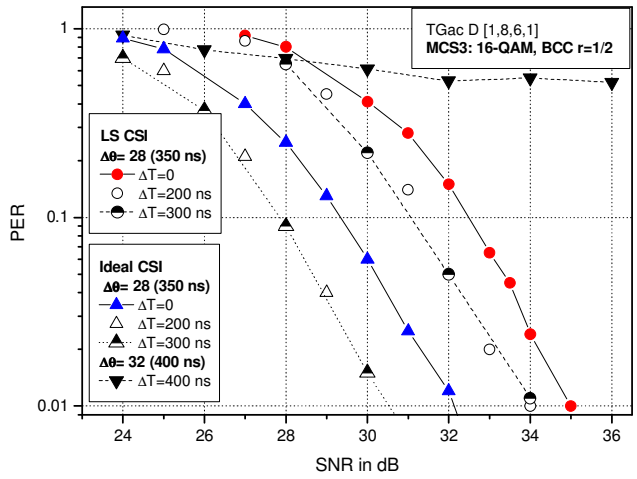

Figure 7. Effects of asynchronous reception on the PER for MCS3 (16-QAM, BCC with code rate ½): [1,8,6,1] TGac D channel; BW=80 MHz; MU-MMSE receiver with LS CSI, MPDU payload of 1500 bytes; soft-decision Viterbi decoding.

the AP [16, pp. 197-198]. The maintenance of the TSF is accomplished as follows: the AP transmits the AP timer in the timestamp field of *Beacons* and *Probe Response Frames*. The STAs associated with the AP utilize this receiving time value, adding a small offset to take into account the MAC layer and PHY processing time.

The time advance proposed in this paper for each client to synchronize the UL MU-MIMO channel is calculated as follows: the control frames transmitted from clients to the AP in any single-user (SU) transmission contain the value of the TSF that informs when this control frame was transmitted. The AP estimates the received TSF using the synchronization scheme (see Eq. 2) and its own TSF. The difference between the TSF estimated by the AP and the TSF transported in the control frame transmitted by each client is storaged in a table as an estimative of the channel delay between the client and the AP. Notice that he AP must use SU transmission from the STAs to estimate the frame time arriving since it is not possible to discriminate the arrival time of each individual client in a UL MU-MIMO transmission, as shown in Section III.

We have implemented this time advance scheme in our IEEE 802.11ax simulator. Fig. 9 (assuming a BW=80 MHz; MU-MMSE receiver, MPDU payload of 1500 bytes; soft-decision Viterbi decoding) shows that the proposed algorithm eliminates completely the performance loss due to asynchronous transmissions shown in earlier figures, considering highly different scenarios (i.e., perfect CSI, realistic LS CSI, TGac B and TGac D channels).

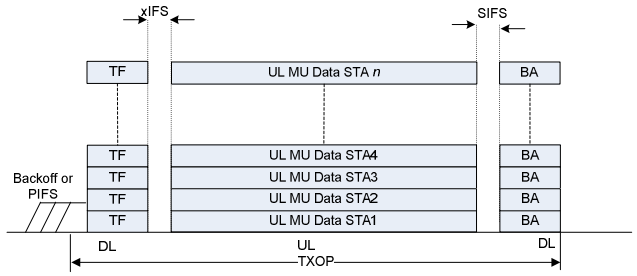

Figure 8. "An example of a transmit opportunity (TXOP) containing an UL MU transmission with an DL MU transmission containing unicast block acknowledgment (BA) frames acknowledging the frames received from the respective STAs". Acronyms: PIFS (Point coordination IFS); TF (Trigger Frame); SIFS (Short IFS) [1, pp. 32].

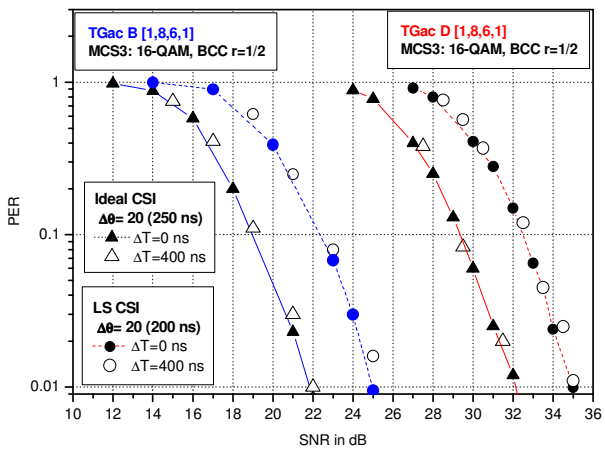

Figure 9. Comparison between the PER for a synchronous channel ($\Delta T = 0\ ns$) with the PER for an asynchronous channel ($\Delta T = 400\ ns$) when the time advance mechanism is implemented. The results for [1,8,1,6] UL-MIMO TGac B and TGac D channels are shown on the left and on the right-side corners, respectively.

V. CONCLUSIONS

First, we have described the present status of the IEEE 802.11ax standardization process. Second, we have developed interrelations between the temporal synchronization and intercarrier interference in asynchronous OFDM UL MU-MIMO channels. Next, we have shown that the asynchronous reception can degrade dramatically the performance of UL MU-MIMO 802.11ax PHY. Finally, we have defined and evaluated the performance of a time advance scheme that counterbalance the asynchronous latency in UL MU-MIMO 802.11ax PHY.

REFERENCES

[1] R. Stacey. *Proposed TGax Draft Specification.* IEEE 802.11-16/0024r1, March 2016.

[2] R. Stacey. *Specification Framework for TGax*. IEEE 11-15/0132r15, Jan. 2016.

[3] R. V. Nee et. al.*UL MU-MIMO for 11ac*. IEEE 802.11-09/0852-00-00ac, July, 2009.

[4] R. V. Nee. *Uplink MU-MIMO Sensitivity to Power Differences and Synchronization Errors*. IEEE 802.11-09/1036-00-00ac, Sept. 2009.

[5] R. P. F. Hoefel. "IEEE 802.11ax: A study on techniques to mitigate the frequency offset in the uplink multi-user MIMO", in *8th 2016 IEEE Latin-American Conference on Communication (LATINCOM 2016),* Medellin, Colombia, Nov. 2016.

[6] N. Shah et. al. "Carrier frequency offset correction for uplink multi-user MIMO for next generation Wi-Fi," *in 2015 International Conference on Computing, Networking and Communications*, Anaheim, USA, Fed. 2015.

[7] F. Jiang, R. Porat and T. Mguyen. "On the impact of residual CFO in UL MU-MIMO," *in 2016 IEEE International Conference on Acoustics, Speech and Signal Processing (ICASSP),* Shanghai, March, 2016

[8] R. P. F. Hoefel. "IEEE 802.11ax: Effects of IQ mismatching on the performance of uplink multi-user MIMO," in *21th IEEE International ITG Workshop on Smart Antennas (WSA2017),* Berlin, March 2017.

[9] J. Y. Guo and M. Lin. *Verifying 11ax's PAR by UL MU-MIMO*, IEEE 802.11-16/1414r2, Nov. 2016.

[10] Y. Fanget. al. *Synchronization Requeriments.* IEEE 802.11-14/0818r1, July 2014.

[11] E. Perahia and R. Stacey, *Next Generation Wireless LANS: 802.11n and 802.11ac.2th ed*. Cambridge: Cambridge University Press, 2013.

[12] Wireless LAN Medium Access Control and Physical Layer Specifications, Amendment 5: Enhancement for Very High Throughput for Operations in Bands below 6 GHz. IEEE P802.11ac, Dec., 2013.

[13] J. Heiskala and J. Terry, *OFDM Wireless LANs: a Theoretical and Practical Guide.* Indiana: SAMS Publishing, 2001.

[14] R. Spitschka, *Synchronization Algorithms for OFDM Systems Using the Example of WLAN*. Saarbrucken, Germany: VDM Verlag, 2008.

[15] R. P. F. Hoefel. "On the synchronization of IEEE 802.11n devices over frequency selective TGn channel models," *25th Annual Canadian Conference on Electrical and Computer Engineering (CCECE 2012),* Montreal, 2012.

[16] M. S. Gast, *802.11 Wireless Networks*. O'Reilly, 2005.